metals

MDPI

Article

Effect of Trace Be and Sc Additions on the Mechanical Properties of A357 Alloys

Yu-Chih Tzeng [1], Jo-Kuang Nieh [2], Hui-Yun Bor [2] and Sheng-Long Lee [3,*]

1 Department of Power Vehicle and Systems Engineering, CCIT, National Defense University, Taoyuan 320-338, Taiwan; s933003@hotmail.com
2 Materials and Electro-Optics Research Division, National Chung-Shan Institute of Science and Technology, Taoyuan 320-338, Taiwan; rao.kwang@msa.hinet.net (J.-K.N.); borhy.h12@msa.hinet.net (H.-Y.B.)
3 Department of Mechanical Engineering, National Central University, Taoyuan 320-338, Taiwan
* Correspondence: shenglon@cc.ncu.edu.tw; Tel.: +886-3-4267325

Received: 8 February 2018; Accepted: 17 March 2018; Published: 19 March 2018

Abstract: The effect of the addition of Be and Sc on the microstructure and mechanical properties of A357 alloy were systematically investigated. The results show that the addition of small amounts of Be and Sc could change the acicular structure of iron-bearing intermetallic compounds to harmless compact Al-Fe-Si and Sc-Fe iron-bearing intermetallic compounds. Compact iron-bearing intermetallic compounds could improve fluidity, causing a reduction in interdendritic shrinkage during solidification. The addition of 0.05 wt % Be enhanced the quality index of the A357 alloy by 11% and increased the notch-yield ratio of fracture toughness by 4.5%. In contrast, the addition of 0.05 wt % Sc increased the quality index and the notch to yield ratio of fracture toughness up to 17% and 9%, respectively. Therefore, the microstructure and mechanical properties of the A357 alloy could be improved by substituting Be with Sc.

Keywords: A357 alloy; scandium; microstructure; mechanical properties

1. Introduction

A357 alloy is a hypoeutectic Al-7Si alloy that has been widely used as a component in the automotive and aerospace industries because of its good castability and weldability, high specific strength, and other positive attributes [1,2]. Iron is a common impurity in Al-Si alloys; it readily forms intermetallic compounds with aluminum, silicon, and other elements [3]. Among the iron-bearing intermetallic compounds, β-Al_5FeSi is commonly found in the Al-Si alloy; because of its acicular shape, it easily damages the ductility of the alloy. Therefore, it is common to dope this alloy with neutralizing agents, such as manganese, cobalt, and beryllium, in order to transform the acicular iron-bearing intermetallic compounds into Chinese script or globular/compact shapes that are less harmful to the ductility of the alloy [4–8].

Scandium is an alternative and beneficial additive for Al alloys that causes the formation of an Al_3Sc phase, which restricts the movement of dislocations and retards recrystallization [9]. Quenching the solid solution of the Al-Sc alloy at 640 °C was followed by aging treatment at 350 °C, enabling a stable and intensive precipitation of Al_3Sc for precipitation hardening in order to improve the mechanical properties of the alloy [10]. Adding scandium into aluminum alloys also provided a significant grain refinement effect [11,12]. Although Sc enhances many properties of aluminum alloys, there have been few discussions related to the effects of Sc addition on the iron-bearing intermetallic compounds of Al-Si alloy in the literature. Moreover, A357 alloy contains traces of beryllium (according to ASTM specifications), which is classified as a Category I carcinogen, hence its use is very limited. Therefore, this study investigated the effect of Be and Sc on the iron-bearing intermetallic compounds of A357 alloy via mechanical properties testing and microstructure characterization in order to clarify the

mechanical mechanisms affected by the Be or Sc addition; simultaneously, the feasibility of replacing Be with Sc without degrading the mechanical properties of the A357 alloy was evaluated.

2. Materials and Methods

Strontium-containing alloy A356 ingots were cut into smaller pieces, cleaned, dried, and melted in charges of 20 kg each to prepare the required alloy. Using this base alloy, three main sets of alloys were prepared, corresponding to the additions of suitable amounts of Si and Mg with or without master alloys of Al-10% Be and Al-1.12% Sc. The melting process was carried out in an electrical resistance furnace. The alloy was melted at 760 °C under a protective atmosphere. The melts were degassed using pure Ar gas for 30 min and then poured into a preheated (400 °C) steel metallic mold with dimensions of 125 mm × 100 mm × 25 mm to complete the casting process. Table 1 presents the chemical compositions of the studied alloys, which were determined using an optical emission spectrometer. Alloy A (Al-7Si-0.6Mg), 0.05 wt % Be-containing alloy B (Al-7Si-0.6Mg-0.05Be) and 0.05 wt % Sc-containing alloy C (Al-7Si-0.6Mg-0.05Sc) notation is used to distinguish the three sets of alloys. For the heat treatment processing of the specimen, we adopted T6 heat treatment. According T6 heat treatment specifications, first the specimens were subjected at 540 °C for 10 h of solution treatment; then the specimens was quenched in water at room temperature; finally, the specimens were aged at 160 °C for 6 h.

Table 1. Chemical compositions of the experimental alloys (wt %).

Alloy	Si	Mg	Fe	Sr	Be	Sc	Ti	Al
A	6.97	0.62	0.10	0.014	N.D.	N.D.	0.10	Bal.
B	7.02	0.62	0.10	0.015	0.05	N.D.	0.10	Bal.
C	6.96	0.63	0.10	0.015	N.D.	0.05	0.11	Bal.

N.D.: Not detectable; Bal.: balance.

Electron probe microanalysis (EPMA, JEOL JXA-8500F, JEOL, Tokyo, Japan) in conjunction with wavelength dispersive spectroscopic analyzer operating at 15 KV and 20 nA was used for the chemical analysis of the different phases. Metallographic samples were etched with 0.5% HF solution for 30 s. A dual-beam focused ion beam (FIB, Versa 3D FEI, FEI, Tokyo, Japan) was used to prepare the TEM (Transmission electron microscope) specimens. Using ImageJ 1.45 s software for image analysis, 30 different regions each with an area of 46,563 μm^2 were sampled in order to quantify the aspect ratio and areas of eutectic silicon and iron-bearing phases.

For mechanical properties, the specimens were cut transversely at 200 mm from the bottom of the castings. The mechanical properties testing was conducted using an MTS-810 tensile tester with an initial velocity of 0.2 mm/min. Tensile testing was conducted according to ASTM B557M specifications. In addition, the sharp-notch tension testing on cylindrical specimens was carried out in accordance with the ASTM E602 specification. The notch tensile strength was calculated by dividing the ultimate tensile strength by the original net cross-sectional area of 63.05 mm^2.

3. Results

3.1. Microstructures

The BSE (Back-scattered electron) micrographs of the as-cast alloys A, B, and C combined with the energy dispersive spectrometry of the selected regions are shown in Figure 1 and Table 2, exploring the corresponding iron-bearing intermetallic compounds dispersed in the matrix. The Secondary Dendrite Arm Spacing (SDAS) can be obtained by changing the speed of the cooling medium (air for production of alloy with coarse SDAS) [13]. The secondary dendrite arm spacing (SDAS) of as-cast alloys A, B, and C was found to be between 30–50 um when air furnace speeds were used. The acicular and Chinese-script shape of iron-bearing intermetallic compounds in alloy A (Figure 1a) were confirmed

to be β-Al_5FeSi and $Al_8Mg_3FeSi_6$, respectively. The compact iron-bearing intermetallic compounds in alloy B (Be-containing) shown in Figure 1b was identified as a $Al_7Si_2Fe_3$ phase. Many compact iron-bearing phases, especially $Al_{12}Si_6Fe_2(Mg,Sc)_5$, were present in alloy C, as shown in Figure 1c. These phases were determined to be Sc-Fe with a total Sc and Mg content of 19.8 wt % [12].

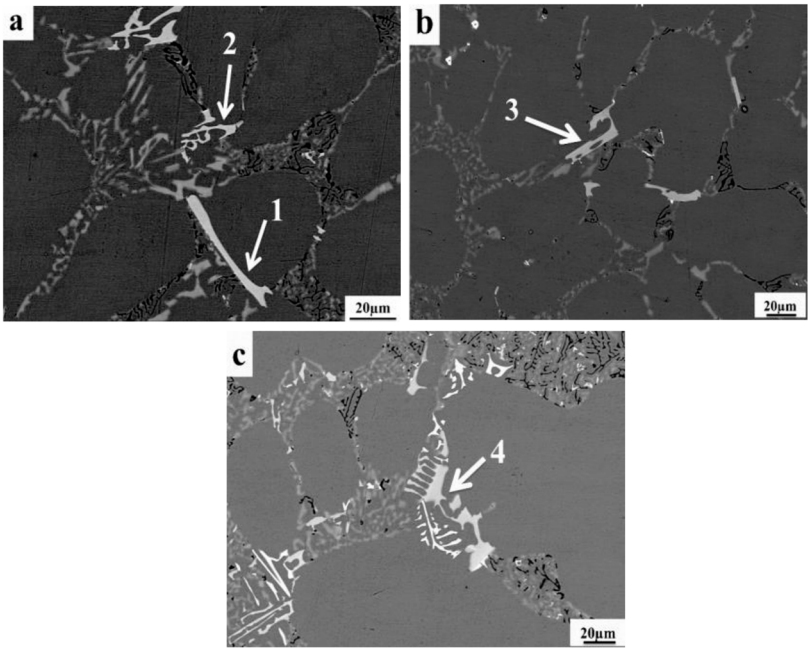

Figure 1. Back-scattered electron micrographs of as-cast alloys: (**a**) alloy A; (**b**) alloy B; and (**c**) alloy C. The arrows indicate (1) acicular Al_5FeSi, (2) π-$Al_8Mg_3FeSi_6$, (3) $Al_7Si_2Fe_3$, and (4) $Al_{12}Si_6Fe_2(Mg,Sc)_5$.

Table 2. Chemical compositions of the intermetallic compounds (wt %).

Marked in Figure 1	Phase	Modular Formula	Al	Fe	Si	Mg	Sc
1	β-Fe	Al_5FeSi	60.8	28.2	10.6	N.D.	N.D.
2	π-Fe	$Al_8Mg_3FeSi_6$	46.5	9.0	26.7	17.8	N.D.
3	Al-Fe-Si	$Al_7Si_2Fe_3$	64.3	26.9	9.6	N.D.	N.D.
4	Sc-Fe	$Al_{12}Si_6Fe_2(Mg,Sc)_5$	46.7	8.0	25.6	19.8	

N.D.: Not detectable.

The acicular β-Al_5SiFe form in Al-Si alloy depends on the alloy chemistry and, more specifically, the Fe level. At high levels of Fe, acicular β-Al_5FeSi tends to form through a binary eutectic reaction with Al, whereas at low Fe levels, it forms in a ternary eutectic reaction with both Al and Si. In the present work, Al, Fe, and Si react with each other in the melt containing no Sc content as follows:

$$L \rightarrow \alpha\text{-Al} + Al_{15}Fe_3Si_2 + (Si) \quad (1)$$

$$L + Al_3Fe \rightarrow \alpha\text{-Al} + Al_{15}Fe_3Si_2 \quad (2)$$

$$L + Al_{15}Fe_3Si_2 \rightarrow \alpha\text{-Al} + Al_5FeSi \quad (3)$$

$$L \rightarrow \alpha\text{-Al} + Al_5FeSi + Si \quad (4)$$

$$L + Al_5FeSi \rightarrow \alpha\text{-Al} + Si + Al_8Si_6Mg_3Fe \quad (5)$$

The final result of the reactions above was the script π phase ($Al_8Si_6Mg_3Fe$). Therefore, it is inferred that when the alloy cools down from a high temperature to the fifth reaction equation above, the solid solution of Sc atoms in $Al_8Si_6Mg_3Fe$ phase replaces some of the Mg atoms with Sc atoms,

thus hindering the distribution of Mg atoms in the $Al_8Si_6Mg_3Fe$ phase. The growth of the $Al_8Si_6Mg_3Fe$ phase along the preferential direction is slowed down, causing the alphabet-like $Al_8Si_6Mg_3Fe$ phase to turn into the spherical $Al_{12}Si_6Fe_2(Mg,Sc)_5$ phase.

The Al-Si-Mg alloy is primarily strengthened by the precipitation of the metastable Mg_2Si phase. During aging, the metastable Mg_2Si precipitates out as finely dispersed phases which anchor the matrix and impede deformation, resulting in a significant increase in strength. Bright-field TEM images of T6-treated alloys A, B, and C are shown in Figure 2. It is remarkable that the needle-shaped β′-Mg_2Si precipitates out as finely dispersed phases, with a length of 50–100 nm, distributed throughout the matrix of alloys A, B, and C. The needle-shaped β′-Mg_2Si precipitates are also coherent with the matrix (as shown in Figure 2b). In contrast, in alloy C (Figure 2d), the Al_3Sc phase was not found, as the T6 heat treatment was not sufficient to induce the precipitation of the Al_3Sc phase [14].

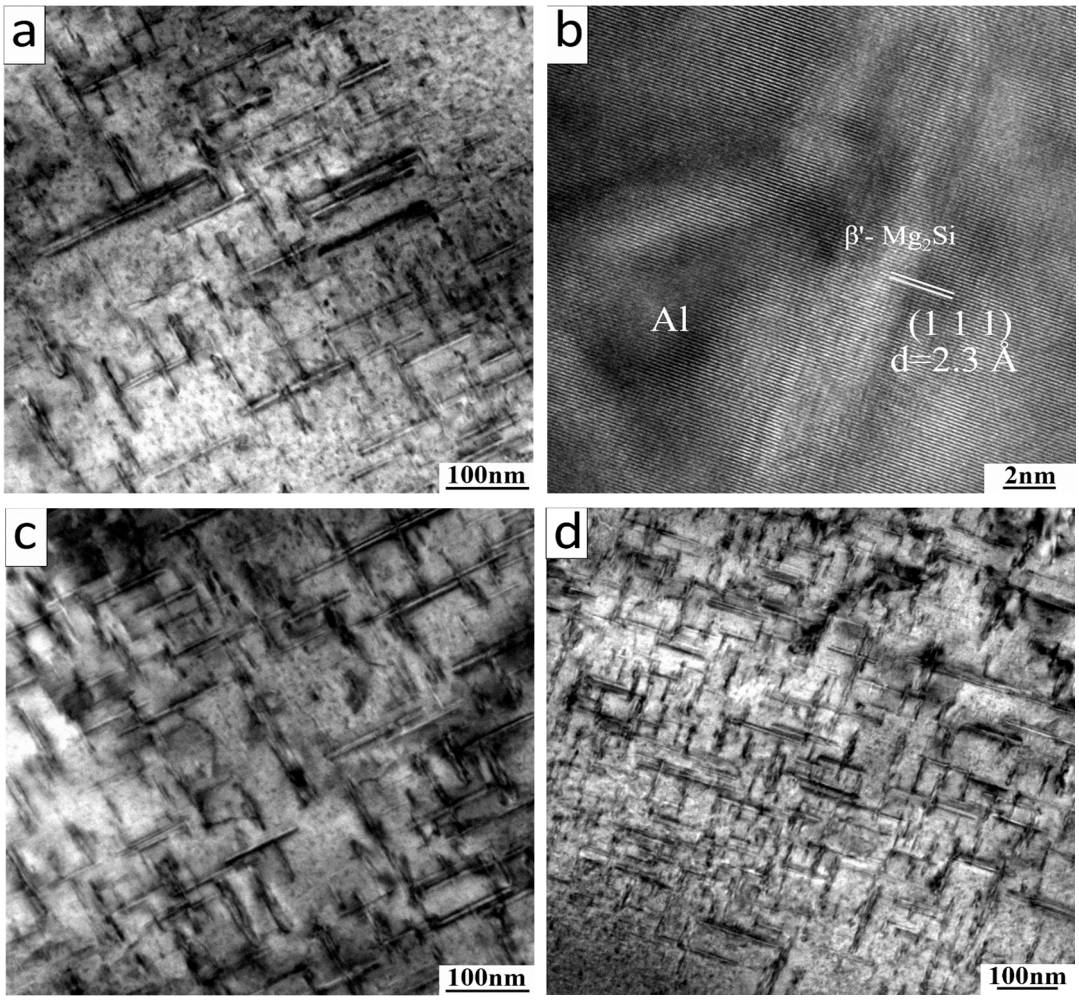

Figure 2. TEM micrographs showing β″-Mg_2Si precipitates in the α-Al matrix of the T6-treated alloys: (**a**) alloy A; (**b**) β′-Mg_2Si precipitates coherent with the matrix; (**c**) alloy B; and (**d**) alloy C.

An image analysis system was used to characterize the geometric parameters and determine the percentages of the eutectic silicon phases and the iron-bearing intermetallic compounds. As shown in Table 3, the eutectic silicon phase morphology shows that a lower eutectic silicon total area percentage and a higher eutectic silicon phase count were found in alloy B than in the alloys A and C. The addition of Be can lower the eutectic melting point, which implies a higher nucleation rate and a finer eutectic silicon phase structure [5]. On the other hand, the addition of 0.05 wt % Sc did not modify the eutectic silicon. However, the total areas occupied by the iron-bearing intermetallic

compounds in alloys B and C were approximately 0.52% and 0.56%, respectively, whereas the total area was approximately 1.24% in alloy A. This result reveals that adding Be or Sc to the A357 alloy converts the morphology of the acicular β-Al_5FeSi phase into compact and harmless compact shapes, subsequently decreasing the amount of iron-bearing intermetallic compounds.

From the microstructural evidence, we found that adding Be to the A357 alloy spheroidized and refined the eutectic silicon phases, but adding 0.05 wt % Sc had no significant effect on the eutectic silicon. However, adding Be and Sc neutralized the embrittling effect on the iron-bearing intermetallic compounds by modifying the acicular morphology to a less harmful and more compact form.

Table 3. Image analysis of silicon particles and iron-bearing intermetallic compounds.

Alloy	Si_p Area (μm^2)	Si_p Count	Si_p Total Area pct	Si_p Aspect Ratio	Iron-Bearing Total Area pct
A	16.1 (0.4)	71 (4)	17.2 (1.1)	1.56 (0.02)	1.24 (0.16)
B	15.7 (0.2)	83 (6)	15.1 (0.7)	1.49 (0.04)	0.52 (0.14)
C	16.3 (0.3)	72 (5)	17.1 (0.7)	1.55 (0.03)	0.56 (0.12)

Standard deviations are listed in parentheses; Si_p: silicon particles.

3.2. Mechanical Properties

Table 4 compiles the results of the mechanical properties testing of alloys A, B, and C under T6 condition, where the quality index ($Q = UTS + 150 \log (EL.)$) is an indicator for both the elongation and tensile strength of the material [15]. According to the previous discussion on the microstructures, it is known that Be can transform the acicular iron-bearing intermetallic compounds into a compact iron-bearing intermetallic compounds that is relatively innocuous to elongation. The addition of Be also slightly decreased the formation of interdendritic shrinkage pores and possessed higher Mg_2Si precipitation during the T6 heat treatment. Therefore, the ultimate tensile strength of alloy B increased to 319 MPa and the elongation of alloy A increased from 3.9% to 5.6%. Because of the improved tensile strength and ductility, the quality index also increased by 11%. Similarly, Sc was able to transform the coarse, acicular β-Al_5FeSi iron-bearing phase into the relatively small, compact Sc-Fe iron-bearing phase, and was also able to effectively reduce the formation of interdendritic shrinkage. Thus, the elongation of alloy C increased dramatically to 8.4%. The larger plastic deformations produced greater hardening, increasing the ultimate tensile strength and quality index to 317 MPa and 17%, respectively. Because the hard brittle iron-bearing intermetallic compounds impede the natural plastic flow of the matrix (molten Al) surrounding them, the shrinkages nucleated by these inclusions coalesce and grow under the applied stress, leading to the formation of a final fracture. This is an explanation why alloy C, with less shrinkage, has a much higher value of elongation than alloys A and B.

Table 4. Mechanical properties of alloys A, B, and C after T6 heat treatment.

Properties Alloys	*YS* (MPa)	*UTS* (MPa)	*EL.* (%)	*Q* (MPa)	Notch Tensile Strength (MPa)	Notch to Yield Ratio
A	250 (5)	300 (5)	3.9 (0.8)	388	333 (4)	1.33
B	255 (2)	319 (3)	5.6 (0.4)	431	355 (5)	1.39
C	248 (4)	317 (5)	8.4 (0.5)	455	362 (4)	1.45

Standard deviations are listed in parentheses.

Figure 3 shows the fracture surfaces of alloys A, B, and C after T6 heat treatment as tensile specimens. Figure 3a shows the distribution of interdendritic shrinkage in alloy A. The presence of interdendritic shrinkage decreased significantly on the fracture surface of the alloy. The fractograph of alloy C, shown in Figure 3c, reveals that there is almost no interdendritic shrinkage. Interdendritic shrinkage occurs due to inadequate flow of liquid aluminum and has no relation to heat treatment or the application of external forces. Moreover, the area of a shrinkage pore is directly proportional to the amount and size of the iron-bearing intermetallic compounds [16]. The image analysis of the shrinkage area of the fracture surfaces of alloys A, B, and C suggested that the shrinkage area of the acicular β-Al_5FeSi-containing alloy A was 1.45%. For alloy B, in which the acicular iron-bearing intermetallic compounds were modified into more flow-conductive compact structures, the area decreased to 0.93%. However, the shrinkage area of alloy C, which contained the compact Sc-Fe iron-bearing intermetallic compounds, decreased drastically to 0.36% because of the smaller interference on the fluidity of molten Al.

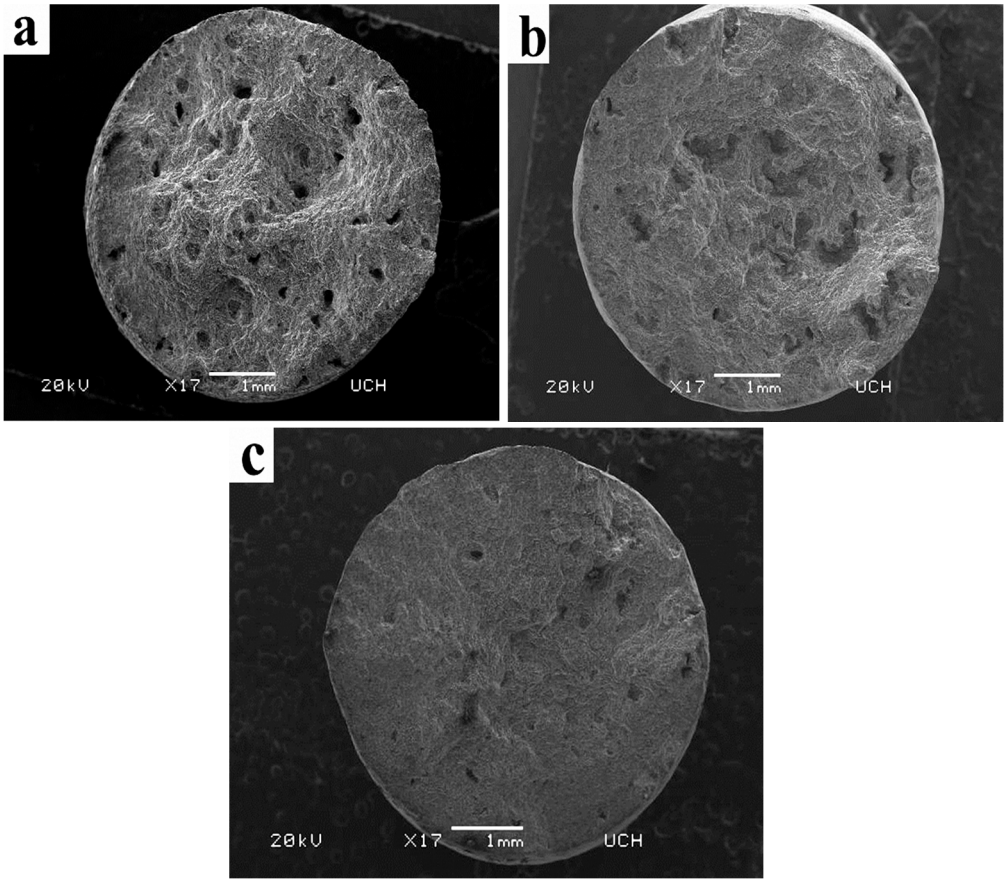

Figure 3. SEM fractographs of the tensile specimens: (**a**) alloy A; (**b**) alloy B; and (**c**) alloy C.

Figure 4a shows the interdendritic shrinkage on the fracture surface of alloy A. The existence of acicular intermetallic compounds in the shrinkage area is shown in Figure 4b. Similarly, the compact iron-bearing intermetallic compounds of alloy B are evident in Figure 4c. The above phenomenon explains how the iron-bearing plate constitutes a potential barrier for liquid metal feeding into the casting region subjected to shrinkage. Specifically, the flow of molten aluminum was hindered. The poor fillability resulted in the formation of interdendritic shrinkages due to an insufficient supply of molten aluminum. However, the addition of Sc may have promoted the formation of a Sc-Fe phase ($Al_{12}Si_6Fe_2(Mg,Sc)_5$), while suppressing the formation of a β-Al_5FeSi phase. The number of obstacles to block the flow of molten aluminum was thus reduced. Prukkanon noted that the addition

of Sc to the Al-7Si-0.3Mg alloy increased the fluidity of the molten aluminum [17]. Therefore, alloy C (Sc-containing) had fewer shrinkage pores and hence significantly enhanced ductility in comparison to alloy A.

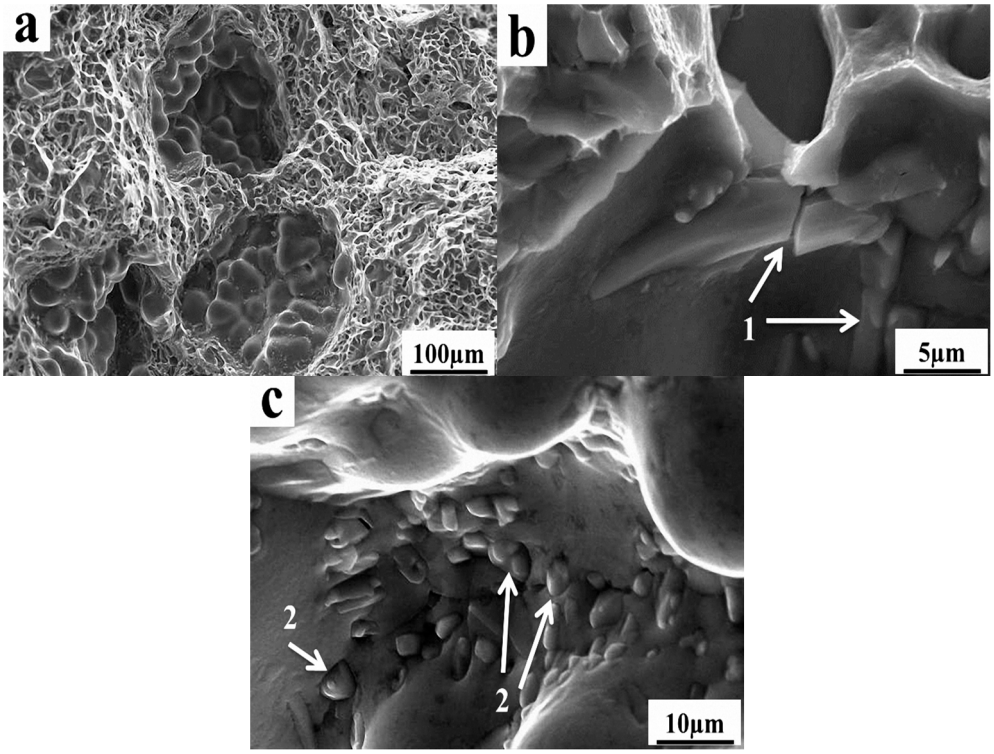

Figure 4. SEM micrographs identifying the particles associated with the shrinkage formation area of the iron-bearing phase: (**a**) interdendritic shrinkage of alloy A; (**b**) magnified interdendritic shrinkage of alloy A; and (**c**) interdendritic shrinkage of alloy B. The arrows in 1 and 2 indicate the acicular and compact iron-bearing phases, respectively.

Table 4 also shows the results for the sharp-notch tensile testing of alloys A, B, and C under the T6 heat treatment condition. The purpose of the sharp-notch tensile test was to calculate the NTS (notch tensile strength) value of the alloys. This ratio (notch to yield ratio, NYR) of notch tensile strength to tensile yield strength has been shown to provide data which correlate well with plane strain fracture toughness. The notch to yield ratio can be used to evaluate the ability of a material to resist fractures initiated by the development of plastic deformation at severe stress concentrations. A greater notch to yield ratio implies a greater amount of plastic deformation before fracture. As discussed previously, Be and Sc improved the morphology of the acicular iron-bearing intermetallic compound by transforming them into compact shapes. In addition, Sc more effectively reduced the number of shrinkage cavities during alloy solidification. Hence, it was not surprising that the notch to yield ratio of alloy B (Be-containing) (1.39) was greater than that of alloy A (1.33), while that of alloy C (Sc-containing) was even greater (1.45).

From the notch tensile fracture surface of alloy A in Figure 5a, mainly smooth and bright cleavage planes, accompanied by small dimples, were found on the fracture surface. Therefore, when alloy A is under stress concentration, the rupture mechanism is mainly based on brittle fracture. For alloy B, in Figure 5b, a mixture of cleavage planes and dimple tissues was found on the surface. For alloy C, in Figure 5c, a mixture of the cleavage planes and dimples was observed, with the dimples tending to be more densely distributed. These formations imply that when alloy B and alloy C are under stress concentration, the rupture mechanism tends to be ductile fracture.

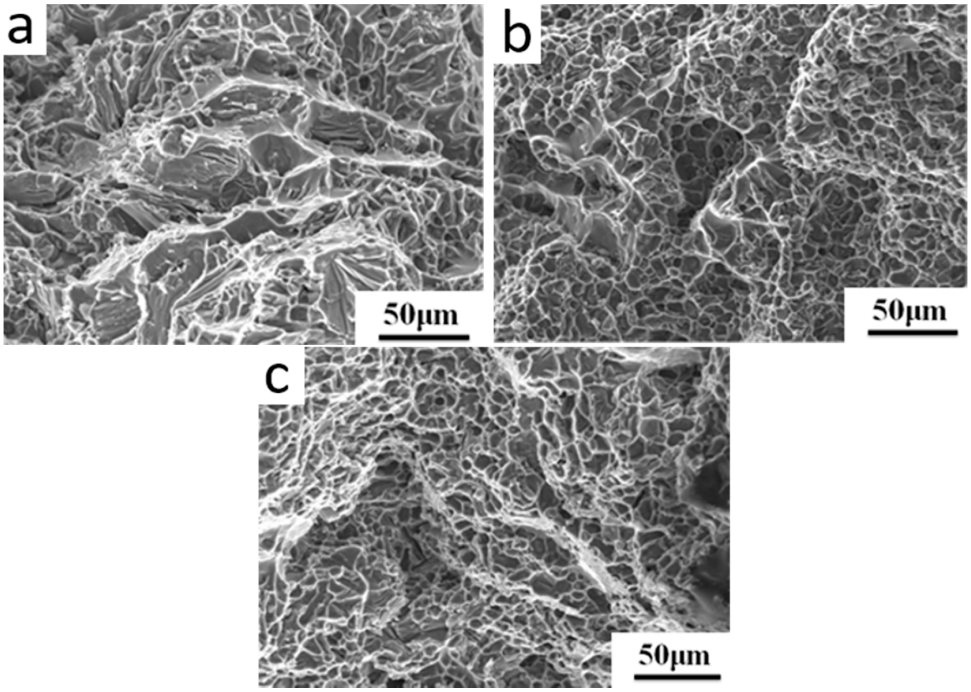

Figure 5. SEM fractograph of the notch tensile specimens: (**a**) alloy A; (**b**) alloy B; and (**c**) alloy C.

4. Conclusions

In this study, the addition of Be and Sc to the A357 alloy and their effect on the alloy's mechanical properties were investigated. The results are summarized below:

(1) Iron-bearing intermetallic compounds with acicular shapes were found in the A357 alloy without Be or Sc addition. These structures were replaced by compact iron-bearing intermetallic compounds when Be or Sc were added.
(2) Adding Be transformed the coarse and acicular iron-bearing phase into a fine compact Al-Fe-Si iron-bearing intermetallic compound, simultaneously reducing interdendritic shrinkage.
(3) Adding Sc significantly enhanced the mechanical properties of the alloys by transforming the coarse and acicular iron-bearing intermetallic compound into a finer, compact Sc-Fe iron-bearing intermetallic compound, and by effectively reducing interdendritic shrinkage.
(4) Adding 0.05 wt % Sc to 357 alloy significantly improved its mechanical properties. The effect was superior to adding 0.05 wt % Be. Therefore, Sc can replace Be to improve the mechanical properties of the alloy.

Acknowledgments: This work was supported by the National Chung-Shan Institute of Science and Technology Grant Number NCSIST-1164-V202(107).

Author Contributions: Yu-Chih Tzeng wrote the paper; Jo-Kuang Nieh measured the silicon particles and iron-bearing intermetallic compounds; Hui-Yun Bora conducted research on SEM micrographs; Sheng-Long Lee managed the experimental work and made correction on the article.

Conflicts of Interest: The authors declare no conflict of interest.

References

1. Sha, G.; Möller, H.; Stumpf, W.E.; Xia, J.H.; Govender, G.; Ringer, S.P. Solute nanostructures and their strengthening effects in Al-7Si-0.6Mg alloy F357. *Acta Mater.* **2012**, *60*, 692–701. [CrossRef]
2. Zykova, A.; Kazantseva, L.; Popova, N.; Vorozhtsov, A.; Kurzina, I. Influence of modifying mixtures on Si crystal Formation in Al-7% Si Alloy. *Metals* **2018**, *8*, 98. [CrossRef]

3. Bjurenstedt, A.; Seifeddine, S.; Jarfors, A.E.W. The Effects of Fe-particles on the tensile properties of Al-Si-Cu Alloys. *Metals* **2016**, *6*, 314. [CrossRef]
4. Shabestari, S.G.; Mahmudi, M.; Emamy, M.; Campbell, J. Effect of Mn and Sr on intermetallics in Fe-rich eutectic Al-Si alloy. *Int. J. Cast Met. Res.* **2002**, *15*, 17–24. [CrossRef]
5. Tan, Y.H.; Lee, S.L.; Lin, Y.L. Effects of Be and Fe content on plane strain fracture toughness in A357 alloys. *Metall. Mater. Trans. A* **1995**, *26*, 2937–2945. [CrossRef]
6. Wang, P.S.; Lee, S.L.; Lin, J.C.; Jahn, M.T. Effects of solution temperature on mechanical properties of 319.0 aluminum casting alloys containing trace beryllium. *J. Mater. Res.* **2000**, *15*, 2027–2035. [CrossRef]
7. Yang, C.Y.; Lee, S.L.; Lee, C.K.; Lin, J.C. Effects of Be and Fe on the mechanical and corrosion behaviors of A357 alloys. *Mater. Chem. Phys.* **2005**, *93*, 412–419. [CrossRef]
8. Murali, S.; Raman, K.S.; Murthy, K.S.S. Morphological studies on β-Al_5FeSi phase in Al-7Si-0.3Mg alloy with trace additions of Be, Mn, Cr, and Co. *Mater. Charact.* **1994**, *33*, 99–112. [CrossRef]
9. Costa, S.; Puga, H.; Barbosa, J.; Pinto, A.M.P. The effect of Sc additions on the microstructure and age hardening behavior of as cast Al-Sc alloys. *Mater. Des.* **2012**, *42*, 347–352. [CrossRef]
10. Marquis, E.A.; Seidman, D.N. Nanoscale structural evolution of Al_3Sc precipitation in Al(Sc) alloys. *Acta Mater.* **2001**, *49*, 1909–1919. [CrossRef]
11. Patakham, U.; Kajornchaiyakul, J.; Limmaneevichitr, C. Grain refinement mechanism in an Al-Si-Mg alloy with scandium. *J. Alloys Compd.* **2012**, *542*, 177–186. [CrossRef]
12. Tzeng, Y.C.; Wu, C.T.; Bor, H.Y.; Horng, J.L.; Tsai, M.L.; Lee, S.L. Effects of scandium addition on iron-bearing phases and tensile properties of Al-7Si-0.6Mg alloys. *Mater. Sci. Eng. A Struct.* **2014**, *593*, 103–110. [CrossRef]
13. Ceschini, L.; Morri, A.; Toschi, S.; Johansson, S.; Seifeddine, S. Microstructural and mechanical properties characterization of heat treated and overaged cast A354 alloy with various SDAS at room and elevated temperature. *Mater. Sci. Eng. A Struct.* **2015**, *648*, 340–349. [CrossRef]
14. Seidman, D.N.; Marquis, E.A.; Dunand, D.C. Precipitation strengthening at ambient and elevated temperatures of heat-treatable Al(Sc) alloys. *Acta Mater.* **2002**, *50*, 4021–4035. [CrossRef]
15. Drouzy, M.; Jacob, S.; Richard, M. Interpretation of tensile results by means of quality index and probable yield strength. *AFS Int. Cast Met. Res.* **1980**, *5*, 43–50.
16. Moustafa, M.A. Effect of iron content on the formation of β-Al_5FeSi and porosity in Al-Si eutectic alloys. *J. Mater. Process. Technol.* **2009**, *209*, 605–610. [CrossRef]
17. Prukkanon, W.; Srisukhumbowornchai, N.; Limmaneevichitr, C. Influence of Sc modification on the fluidity of an A356 aluminum alloy. *J. Alloys Compd.* **2009**, *487*, 453–457. [CrossRef]